J Incl Phenom Macrocycl Chem
DOI 10.1007/s10847-016-0633-0

ORIGINAL ARTICLE

Docking and physico-chemical properties of α- and β-cyclodextrin complex containing isopulegol: a comparative study

Paula dos Passos Menezes[1] · Grace Anne Azevedo Dória[1] · Adriano Antunes de Souza Araújo[1] · Bruna Maria Hipólito Sousa[1] · Lucindo José Quintans-Júnior[2] · Rafaely Nascimento Lima[3] · Péricles Barreto Alves[3] · Flávio Machado Souza Carvalho[4] · Daniel Pereira Bezerra[5] · Francisco Jaime Bezerra Mendonça-Júnior[6] · Luciana Scotti[7] · Marcus Tullius Scotti[8] · Gabriel Francisco da Silva[9] · Thiago Mendonça de Aquino[10] · Adilson Rodrigues Sabino[10] · Eryvaldo Socrates Tabosa do Egito[11] · Mairim Russo Serafini[1]

Received: 25 February 2016 / Accepted: 4 June 2016

Abstract Isopulegol (ISOP) is a monoterpenoid alcohol presented in the essential oils of several plants that possesses therapeutic properties The aim of this work was prepare samples with ISOP and α- and β-cyclodextrins (α- and β-CD) through three different methods: physical mixture, paste method (PC) and slurry complexation (SC). In order to evaluate the formation of inclusion complexes, the techniques of differential scanning calorimetry, thermogravimetry/derivative thermogravimetry, fourier transform infrared spectroscopy, X-ray diffractometry (XRD), gas chromatography–mass spectrometry analyses (GC/MS), docking, nuclear magnetic resonance and scanning electron microscopy were considered. The analyses of the α-CD or β-CD/ISOP revealed the formation of a complex mainly through the PC and SC methods for α-CD and β-CD, respectively. XRD diffraction characteristics presented formation of a trend to new solid phase, which suggested the formation of inclusion complexes. The GC/MS demonstrated that the PC method was the best one to form complexation with α-CD (48.8 %). Concerning β-CD, the SC method exhibited the strongest complexation (68.3 %). Furthermore, the molecular theoretical docking study demonstrated that α-CD/ISOP inclusion complex formed a more stable complex than did the β-CD/ISOP inclusion complex.

Keywords Cyclodextrin · Inclusion complexes · Isopulegol · Monoterpenoid

✉ Mairim Russo Serafini
paula.dp.menezes@gmail.com

[1] Departamento de Farmácia, Universidade Federal de Sergipe, São Cristóvão, Sergipe, Brazil

[2] Departamento de Fisiologia, Universidade Federal de Sergipe, São Cristóvão, Sergipe, Brazil

[3] Departamento de Química, Universidade Federal de Sergipe, São Cristóvão, Sergipe, Brazil

[4] Departamento de Mineralogia e Geotectônica, Universidade de São Paulo, São Paulo, Brazil

[5] Centro de Pesquisa Gonçalo Moniz, Fundação Oswaldo Cruz, Salvador, Bahia, Brazil

[6] Laboratório de Síntese e Vetorização de Moléculas, Universidade Estadual da Paraíba, Campina Grande, Paraíba, Brazil

[7] Universidade Federal da Paraíba, Campina Grande, Paraíba, Brazil

[8] Departamento de Engenharia e Ambiente, Universidade Federal da Paraíba, Campina Grande, Paraíba, Brazil

[9] Departamento de Engenharia Química, Universidade Federal de Sergipe, São Cristóvão, Sergipe, Brazil

[10] Laboratório de Ressonância Magnética Nuclear, Universidade Federal de Alagoas, Maceió, Alagoas, Brazil

[11] Departamento de Farmácia, Universidade Federal do Rio Grande do Norte, Natal, Rio Grande do Norte, Brazil

Published online: 16 June 2016

Introduction

Terpenoids are secondary metabolites of essential oils, represented mainly by monoterpenes, which account is about 90 % of the essential oils. These are derived from isoprene C5 units joined in a manner head-to-tail two biosynthetic pathways through the intermediate mevalonic acid or 1-deoxy-D-xylulose 5-phosphate [1, 2]. They may be acyclic (myrcene and geraniol), monocyclic (terpineol) and bicyclic compounds (α-pinene and camphor) [3]. ISOP (p-ment-8-en-3-ol) (Fig. 1) is one kind of monoterpenoid alcoholic cyclic presented in the essential oils of several plants, that possesses therapeutic properties [4]. It is also a very important intermediate in the industrial production of (−)-menthol, a widely used substance in pharmaceutical products, agrochemicals, toothpastes and chewing gum [5].

Additionally, ISOP showed anticonvulsant activity and bioprotection effect against pentilenotetrazol-induced seizures. Such actions are possibly related to a positive modulation of a γ-aminobutyric acid receptor ($GABA_A$) and to the antioxidant properties of ISOP. Moreover, ISOP could be useful as a new neuroprotective and anticonvulsant natural agent [6]. ISOP also presented depressant- and anxiolytic-like effects [4].

In vivo studies of toxicity and immunotoxicity have been evaluated with ISOP. This substance has shown low toxicity during 14 days after the administration of a single dose [7] and showed no suppression of antibody-forming cells or primary antibody response [8].

The patent US20130084257 shows that ISOP is effective and safe as the percutaneous absorption of various drugs with low skin irritation promoter [9]. However, its high volatility and undesirable odor limit the application of ISOP in transdermal drug delivery systems. To address these issues, Chen et al. synthesized esters of long chain saturated ISOP by esterification reaction with unsaturated fatty acids and resulting in ISOP promising candidates as transdermal permeation enhancers for clinical drug delivery, with the advantages of high efficiency, low volatility, low skin irritation and toxicity [10]. Chen et al. reported the potential long chain esters of ISOP, synthesized above as an effective permeation enhancer, enhanced pharmacodynamic efficacy as well as feasibility of providing significant quantities of flurbiprofen through the skin in transdermal patches [11].

More than 40 % of new chemical entities are practically insoluble in water [12, 13]. One approach to improve the oral bioavailability of such molecules is the use of nanoparticles formulations [14, 15], microparticles systems [16], cyclodextrins (CDs) [17–22]. CDs are cyclic oligosaccharides formed from subunits of α-, β-, and γ-CDs, which have 6, 7 and 8 glucose units, respectively, arranged in a ring shape [21–23]. The diameter of the central cavity of CDs varies in the following order, α-CD (0.5–0.6 nm), β-CD (0.6–0.8 nm), γ-CD (0.8–1.0 nm) and allows selectivity for the complexation of different types of molecules; therefore, the CDs act as molecular encapsulants [22–24]. Among all the solubility enhancement techniques of oily compounds, inclusion complex formation technique has been employed more precisely to improve the aqueous solubility, dissolution rate, bioavailability of poorly water soluble drugs [13, 25, 26], modification of pharmacokinetics and disposition of the sustained release of drugs and targeted therapy [27].

Considering the pharmacological potential of ISOP, this study aims to elucidate the physico-chemical aspects of its inclusion of this monoterpene into α- and β-CDs.

Materials and methods

Material

Alpha-cyclodextrin 98 % (α-CD), beta-cyclodextrin 97 % (β-CD) and (−)-ISOP 98 % were purchased from Sigma Aldrich.

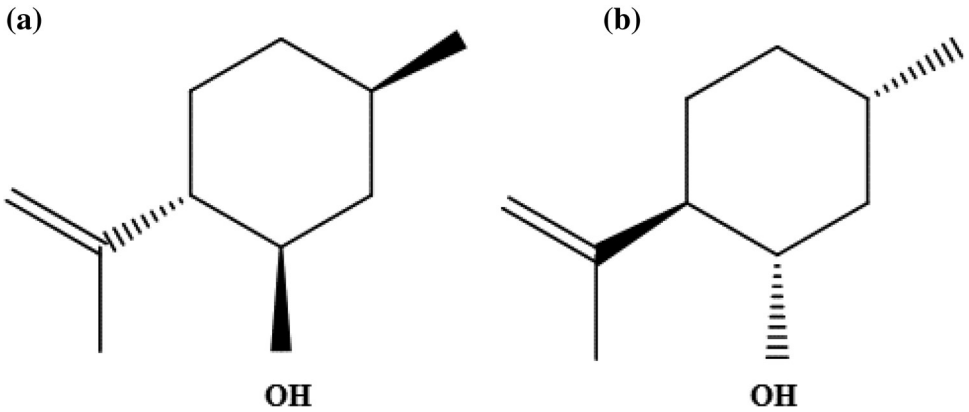

Fig. 1 Molecular structures of **a** (−)-isopulegol and **b** (+)-isopulegol

Preparation of samples

Samples of α-CD/ISOP and β-CD/ISOP were prepared through three different methods: physical mixture (PM), paste complexation (PC) and slurry complexation (SC). The PM samples were prepared by adding ISOP (154 mg) in an agate mortar containing precisely weighed amount of α- (972 mg, based in molecular weight) or β-CD (1135 mg, based in molecular weight) under manual stirring. The ISOP/CD molar ratio was maintained as described for the inclusion complex preparation (1:0.9 for α-CD; 1:0.86 for β-CD). The products were then stored in sealed glass containers. PC was performed through homogenization of α- (972 mg) or β-CD (1135 mg) in 2 mL water directly in an agate mortar. Moreover, the mixture paste was kept under constant manual agitation. Afterwards, the material was dried at room temperature (in a desiccator) until a glass film was formed, which was removed with manual trituration and stored in airtight glass containers. Finally, the SC was carried out by adding water (20 mL) to a beaker containing ISOP (154 mg) and α- or β-CD (1135 mg), under constantly magnetic stirring at 400 rpm for 36 h (Quimis Q 261A21, Brazil). Following, the material was dried in a desiccator and removed with manual trituration as described in the PC method according to Marreto et al. [28].

Thermal analysis

Differential scanning calorimetry (DSC) curves were obtained in a DSC-60 cell (Shimadzu, DSC-60A, USA) performed with aluminum crucibles containing about 2 mg of samples, under dynamic nitrogen atmosphere (50 mL min^{-1}) and heating rate of 10 °C min^{-1} in the temperature range from 25 to 500 °C. The DSC cell was verified with indium (m.p. 156.6 °C; ΔH fus = −28.5 J g^{-1}) and zinc (m.p. 419.6 °C). Thermogravimetry/derivative thermogravimetry (TG/DTG) curves were obtained with a DTG-60 (Shimadzu, DTG-60, USA) thermo-balance in the temperature range of 25–900 °C. The assay was performed with platinum crucibles containing approximately 3 mg of samples, under dynamic nitrogen atmosphere (50 mL min^{-1}) and heating rate of 10 °C min^{-1}. The TG/DTG was verified with calcium oxalate monohydrate, according to the ASTM standard.

Titration of Karl Fisher

The water contents of samples were determined through the Karl Fischer method (Metrohm, 870 KF Titrino Plus, USA) and methanol (Fluka, USA) as titrating solution. The analyses were carried out in triplicate.

Efficiency complexation by gas chromatography–mass spectrometry analyses (GC/MS)

These parameters of this technique were adapted from the study of Marreto et al. [28]. GC analysis was performed using a GC–MS/FID (QP2010 Ultra, Shimadzu Corporation, Kyoto, Japan) equipped with an autosampler AOC-20i auto-injector (Shimadzu). Separations were accomplished using a Rtx®-5MS Restek fused silica capillary column (5 %-diphenyl-95 %-dimethyl polysiloxane) of 30 m × 0.25 mm i.d., 0.25 μm film thickness at a constant helium (99.999 %) flow rate of 1.2 mL min^{-1}. Injection volume of 0.5 μL (5 mg mL^{-1}) was employed, with a split ratio of 1:10. The oven temperature was programed from 50 °C (isothermal for 1.5 min),with an increase of 4 °C min^{-1}–200 °C, then, 10 °C min^{-1}–250 °C, ending with a 5-min isothermal at 250 °C.

The flame ionization detector (FID) and mass spectrometry (MS) data were simultaneously acquired using a detector splitting system; the split flow ratio was 4:1 (MS: FID). A 0.62 m × 0.15 mm i.d restrictor tube (capillary column) was used to connect the splitter to the MS detector. A 0.74 m x 0.22 mm i.d restrictor tube was used to connect the splitter to the FID detector. The MS data (total ion chromatogram, TIC) were acquired in the full scan mode (m/z of 40–350) at a scan rate of 0.3 $scan.s^{-1}$ using the electron ionization with electron energy of 70 eV. The injector temperature was 250 °C and the ion-source temperature was 250 °C. The FID temperature was set at 250 °C and the gas supplies for the FID were hydrogen, air and helium at flow rates of 30, 300 and 30 mL min^{-1}, respectively. Quantification of each constituent was estimated by normalizing the peak area generated in the FID—(%). Compound concentrations were calculated from the GC peak areas and are arranged in order of elution from the GC.

Extraction of total ISOP

Total ISOP adsorbed in the α- or β-CD was determined through extraction according to the method described by Marreto et al. [28]. Distilled water (8 mL), hexane (4 mL) and 0.2 g of the sample were put in a round-bottom flask, which was kept in a water bath at 85 °C for 20 min, with constant shaking. The organic phase was decanted (three times) and concentrated to approximately 1 mL using nitrogen. Afterwards, internal standard (menthol, 2 mg) was added and stored until the GC–MS/FID analysis.

Extraction of surface-adsorbed ISOP

The amount of ISOP adsorbed on the surface of α- or β-CD was determined through washing. The sample (3 g) with

hexane (20 mL) was shaken for 20 min. The suspension was filtered and the residue was washed with hexane (10 mL). Moreover, hexane (1 mL) and internal standard (menthol, 2 mg) were added to the filtrate, which was concentrated using nitrogen and analyzed by means of GC–MS/FID. Thus, the difference between the total ISOP (surface-adsorbed ISOP and hosted in the cavity) and the surface-adsorbed ISOP corresponds to the amount complexed in the α- or β-CD cavity.

Fourier transform infrared (FTIR) spectroscopy

The infrared spectra of ISOP, α- and β-CD, as well as α-CD/ISOP and β-CD/ISOP prepared by three different methods (PM, PC and SC) were evaluated. The FTIR was performed in the range of 4000–500 cm^{-1} in KBr pellets using IRTracer-100 (Shimadzu, IRTracer-100, Japan), at room temperature.

Scanning electron microscopy

The samples were mounted on aluminum stubs, coated with a thin layer of gold and visualized with a scanning electron microscope (JSM-6390-LV JEOL) at an accelerated voltage of 12 kV.

X-ray diffractometry (XRD)

Powder X-ray diffractometer results were obtained on a Rigaku with a tube of CuKa, in the range of 3–65 θ (2θ) and 1 s. of passing time, carried out with the XRD powder method.

Molecular docking between α-, β-CD and ISOP

The chemical structures of the compounds (ISOP and α-, β-CD) were drawn using Marvin 14.9.8.0, 2014, ChemAxon (http://www.chemaxon.com). The software Standardizer, JChem 14.9.8.0, 2014, ChemAxon (http://www.chemaxon.com) was used to canonize the structure, add hydrogens, clean the molecular graph in three dimensions and finally save in .sdf format. The process uses a divide-and-conquer approach. The structure is split into small fragments and is organized into a building tree using its original connectivity information. Conformers generated for the initial structure (represented by the root node in the building tree) are also optimized. The building process uses a proprietary extended version of the Dreiding force field [29].

All the geometry optimization and conformational search were performed using Spartan for Windows 10.0 software [30]. The chemical structure geometry of the compound was initially optimized using the MMFF force field [31] and, afterwards, a new geometry optimization based on the AM1 semi-empirical method (Austin Model 1) was performed [32]. We selected the systematic search method, analyzing up to 1,000 conformers and selecting until 10 conformers of lowest minimum energy using AM1 and the Monte-Carlo algorithm. The dihedrals were evaluated by rotation in accordance with the standard (default) conditions of the program. The conformers of lowest minimum energy were selected and, then, the geometry optimization and vibrational mode calculation using AM1 was performed [32].

The docking simulations were performed on the AutoDock 4.2 software. Receptor and ligand preparation was carried out using a VEGA ZZ 3.0.3 [33] The structures of ligand and receptor were saved in pqbqt format for further use in docking calculations. PyRx 0.9 software-X10 [34] was used to aid the steps of job submission and analysis of the results. A three-dimensional grid box with 50, 44 and 50 points for x, y and z, with a spacing of 0.375 Å, was created. All the other parameters were left at the AutoDock 4.2 default settings [33]. The results for each calculation were analyzed to obtain the affinity energy (Kcal mol^{-1}) values for each ligand conformation in its respective complex and the probable structure inaccuracies were ignored in the calculations. In order to verify the number of hydrogen bonds, hydrophobic interactions and docking interpretation, the program Discovery Studio 4.0 was employed.

Nuclear magnetic resonance (NMR)

^{1}H and H–H 2D NMR analyses were recorded for ISOP, α-CD and β-CD inclusion complexes (prepared through the SC and PC methods) and PM dissolved in D_2O (0.02 M) using a Bruker AVANCE 400 spectrometer. The spectra were acquired at 298 K in 5-mm tubes. Chemical shifts were measured relative to the peak at 4.80 ppm, due to the solvent (D_2O). The ROESY spectrum was recorded applying a mixing time of 500 ms under spin lock condition, 256 increments were collected with 32 repetitions and the data matrix measured was processed as a matrix of 2 k (F2) by 1 k (F1) data points [35].

Results and discussion

Thermal analysis

Thermal analysis of the ISOP, α- and β-CD, physical mixture and α- or β-CD/ISOP revealed the formation of a complex. According to Hădărugă et al., DSC can provide further information on the physical and chemical processes occurring during heating, even if the guest compound is not volatile up to the CD degradation temperature [36]. The

DSC curves of ISOP showed endothermic peaks between 34 and 134 °C corresponding to its volatilization ($\Delta H = -425.75$ J g^{-1}) (Fig. 2a, b). The PM, PC and SC showed a sharp endothermic peak in the range of the volatilization of the pure compound (30–143 °C). The DSC curve of the α-CD (Fig. 2a) indicated two endothermic events. On the first one, in the range of 50–148 °C ($\Delta H = -257.73$ J g^{-1}), three consecutive endothermic events occurred, as described by Giordano et al. [37], which corresponds to the dehydration of the molecule. The second event occurred in the range of 300–355 °C ($\Delta H = -468.55$ J g^{-1}) and this attributed to the fusion followed by the decomposition of the α-CD molecules. The DSC curves of the α-CD/PM indicated two endothermic events: the first one in the range of 38–144 °C (which corresponds to the release of water molecules as well as to the release of ISOP, probably adsorbed on the α-CD surface, $\Delta H = -205.35$ J g^{-1}) and the second one in the range of 312–336 °C ($\Delta H = -443.20$ J g^{-1}), in which the fusion followed by decomposition of α-CD molecules appeared.

The DSC curves for the PC and the SC with α-CD (Fig. 2a) clearly indicated the difference related to the PM, α-CD and ISOP curves alone. The PC and SC curves display two endothermic events, PC at 37–169 °C, $\Delta H = -205.35$ J g^{-1} and 309–339 °C, $\Delta H = -121.45$ J g^{-1} and SC at 50–150 °C, $\Delta H = -95.24$ J g^{-1} and 293–358 °C, $\Delta H = -172.54$ J g^{-1}. The first event showed the release of water and oil. The second event corresponded to the α-CD melting point followed by decomposition, as was showed by the α-CD and PM curves.

The β-CD curve (Fig. 2b) exhibited a broad thermal peak between 32 and 132 °C ($\Delta H = -287.10$ J g^{-1}) that corresponds to the water release [38]. From the range of 215–228 °C ($\Delta H = -1.18$ J g^{-1}) an additional endothermic event occurred, which is characteristic of the crystalline phase transition [39] that disappeared in the PC and SC methods, evidencing the complexation. The presence of a thermal event between 300 and 361 °C ($\Delta H = -264.61$ J g^{-1}) is generally attributed to the fusion followed by the decomposition of the β-CD [40]. The DSC curve of the β-CD/ISOP prepared by PM was similar to

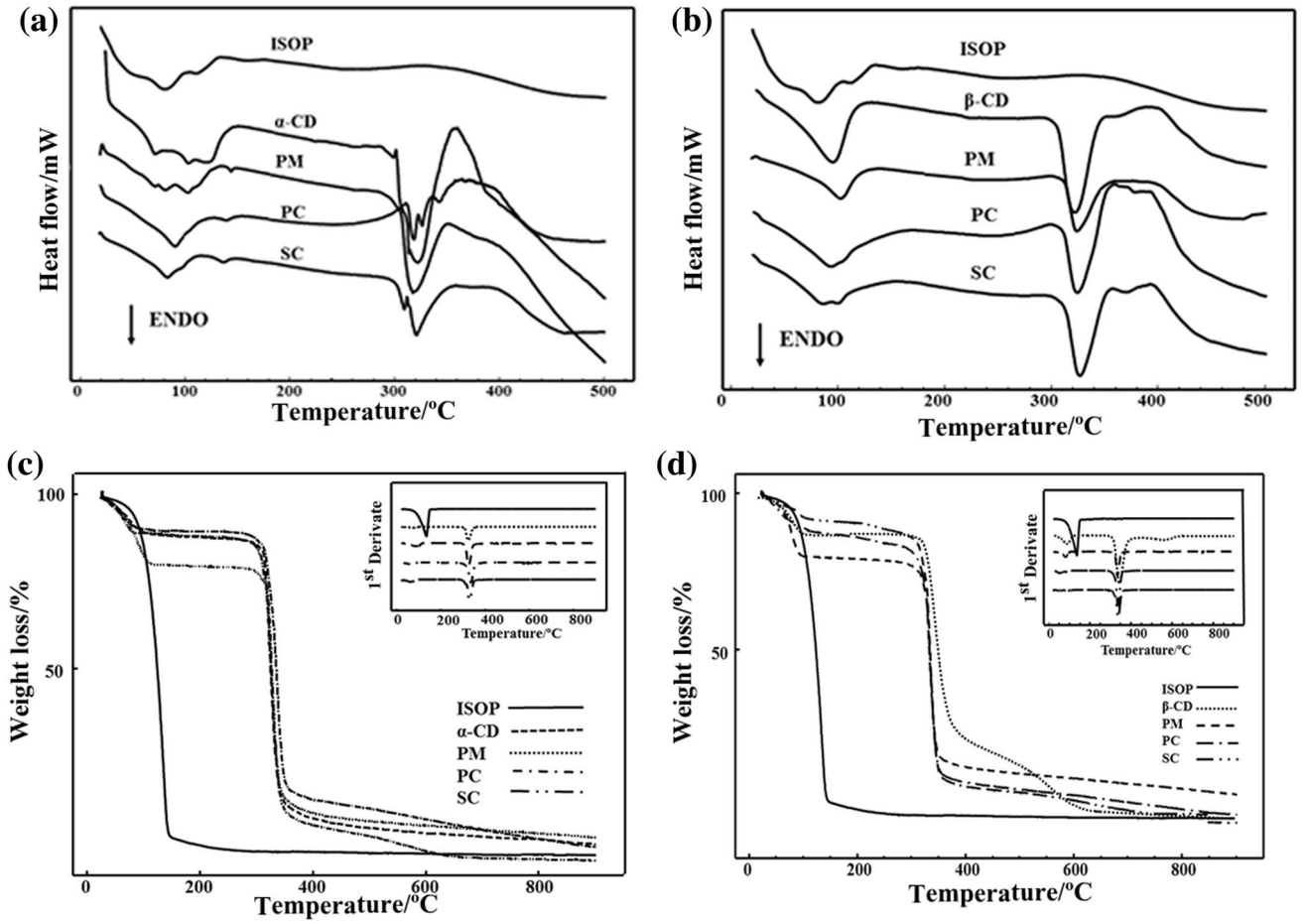

Fig. 2 DSC (**a**, **b**) and TG/DTG (**c**, **d**) curves of ISOP, α–CD, β-CD, physical mixture (PM) and inclusion complex prepared through paste complexation (PC) and slurry complexation (SC) in dynamic nitrogen atmosphere (50 mL min^{-1}) and heat rate of 10 °C min^{-1}

that of pure β-CD, indicating that β-CD was present in its free form in that sample and in the ISOP was adhered to the surface. The β-CD/ISOP prepared through PC and SC showed better interaction of the components. As for α-CD, these curves showed two endothermic events. The first one at 41–161 °C; $\Delta H = -237.40$ J g^{-1} for the PC/β-CD and 45–145 °C; $\Delta H = -159.79$ J g^{-1} for the SC/β-CD attributed to the water and surface oil (ISOP) loss. The second one in the range of 301–353 °C; $\Delta H = -261.00$ J g^{-1} for the PC/β-CD and 300–355 °C; $\Delta H = -224.89$ J g^{-1} for the SC/β-CD characteristic to the β-CD fusion. According to Rajendiran et al. and Castronuovo and Niccoli, the ΔH value suggests the inclusion complex formation between ISOP with β-CD indicating strong interactions between ISOP and the CD cavity in this orientation. The value of enthalpy is the result of several factors, among them the endothermic contribution due to the disruption of the hydrogen bonds between water molecules in the cavity, the endothermic dehydration of the included hydrophobic guest molecule and the exothermic contribution stemming from the van der Waals interactions between the guest and the CD cavity [41, 42]. The host–guest interaction causes an enthalpy–entropy compensating process in the gas phase whereas the same interaction causes an enthalpy–entropy co-driven process in aqueous solution. That is because inclusion complexation releases a number of water molecules from the cavities of CD [43].

The TG/DTG curves of ISOP showed two weight loss steps, which were characteristic of volatilization and decomposition. In the range of 25–146 °C, the oil weight loss was 98.23 % and in the second step (146–166 °C), the oil weight loss was 1.71 % (Fig. 2c, d). These results corroborated with the endothermic event in the DSC curve that represented the volatilization of ISOP. The Table 1 exhibited the range and weight loss of evaluated products (ISOP, α-CD, PM/α-CD, PC/α-CD, SC/α-CD, β-CD, PM/β-CD, PC/β-CD and SC/β-CD). The α-CD alone in the range of 25–111 °C and 111–293 °C had a weight loss of 10.52 and 2.54 %, respectively. The first weight loss is associated to the release of water molecules. Indeed, Giordano et al. [37] described that α-CD has a water loss and structural rearrangements within 30–130 °C with 6.41 % of weight loss. On the other hand, Kohata et al. [44] not only confirmed this founding, but also revealed that, in the range of 260–270 °C, α-CD presented a release of tightly bound water. However, concerning SC/α-CD ($\Delta m = 3.05$ %) complex our results revealed that the second weight loss step was occurred below the temperature of tightly bound water loss of α-CD (260–270 °C), which could be attributed to that the complex formed between ISOP and the α-CD. In fact, in this step, ISOP was completely volatilized up to 166 °C. PM/α-CD and PC/α-CD showed weight loss of 1.93 %, less than α-CD, corresponding to water loss. The TG/DTG curves of β-CD (Fig. 2; Table 1) showed four steps of weight loss. In the first step, from 25 to 111 °C, β-CD lost 11.51 % of water, which is in agreement with other studies performed by our research group [17, 18, 45]. Between 111 and 293 °C, the TG curve was flat and no mass loss was detected. Additionally, the thermal decomposition (around 65.31 %) occurred after 293 °C. Then, a continuous carbonization occurred in a wide temperature range from 421 to about 900 °C ($\Delta m = 21.05$ %). The PM/β-CD, PC/β-CD and SC/β-CD lost 2.44, 5.73 and 5.33 % respectively between 111 and 243 °C. Therefore, the PC/β-CD and SC/β-CD were able to form inclusion complexes, once the loss of the complexed oil in a higher range of temperature when compared to the water release and the volatilization process of the oil from the surface, which happened at 166 °C. Furthermore, the TG technique does not distinguish water and oil in the weight loss. Therefore, in order to assess the water of samples, a Karl Fischer technique assay was performed (Table 1). These results showed that α- and β-CD had 12.25 ± 0.73 and 13.75 ± 0.39 % of water, respectively, while the samples of ISOP and CDs had a variable percentage related to the first step of TG. This could be explained by the amount of oil on the surface of CDs. The Karl Fischer technique is a great tool to evaluate water concentration in CDs and inclusion complexes according to Hădărugă et al. and Hădărugă et al. [36, 46]. In the Table 1, it can be seen that the PM presented major weight loss (water and oil) in the first step. This happened because the oil did not form inclusion complex and remained adsorbed on the surface of CDs. On the other hand, PC and SC methods showed less water loss content in the first step, which is in agreement with the Karl Fischer results in which the content of water of PC and SC. Some authors have described that the formation of the inclusion complex improves the thermal stability of low-solubility molecules [39, 47, 48]. This statement corroborated with foundings of our study, in which it was demonstrated that ISOP can form a stable inclusion complex with CDs.

Del Valle described that oils can be complexed in a solution, but the increase in water amount supports the separation of the oil molecules from such complex and further impeaches the inclusion complexes formation. Therefore, some studies suggested the SC as the best method for inclusion complexes formation [49].

Total and surface oil of α- and β-CD/ISOP complex

The inclusion complex formation prepared through the three different methods was determined by GC–MS, as is given in Table 1. The GC/MS of PM, PC and SC with α-CD and β-CD demonstrated that PC/α-CD was the best method of inclusion complex yelding 48.8 % of complexed

Table 1 Mass losses for ISOP, α-CD, β-CD, PM, PC and SC complexes in different temperature intervals obtained through TG/DTG analyses. Percentage of water in the samples was quantify by the Karl Fischer titration. Gas chromatography–mass spectrometry analyses (GC/MS) performed the efficiency of complexation

Sample	Δm_1/% 25–111 °C	Δm_2/% 111–293 °C	Δm_3/% 293–421 °C	Δm_4/% 421–900 °C	%H_2O	Surface oil (%)	Total oil (%)	ISOP complex (%)	Complexation ratio[b] (%)
ISOP	98.23[a]	1.71[a]	–	–	1.20 ± 0.16	–	–	–	–
α-CD	10.52	2.54	80.31	0.94	12.25 ± 0.73	–	–	–	–
PM/α-CD	18.82	1.94	70.65	6.21	9.82 ± 0.29	76.58	94.72	18.14	1:0.24
PC/α-CD	9.26	1.93	76.32	13.04	8.25 ± 1.16	1.24	61.71	60.47	1:48.8
SC/α-CD	12.02	3.05	81.73	9.32	11.18 ± 1.01	2.77	57.97	55.20	1:19.9
β-CD	11.51	0.83	67.05	21.05	13.75 ± 0.39	–	–	–	–
PM/β-CD	19.26	2.44	65.31	8.23	14.56 ± 0.85	64.31	77.81	13.50	1:0.2
PC/β-CD	10.41	5.73	75.25	9.54	8.06 ± 0.76	15.41	66.92	51.51	1:3.3
SC/β-CD	6.85	5.33	80.42	8.84	12.465 ± 0.71	0.86	59.62	58.76	1:68.3

[a] The range of weight loss for ISOP was 25–146 and 146–166 °C. For the other samples, it was 25–111, 111–293, 293–421 and 421–900 °C, respectively in accordance to the subtitle of the table

[b] Ratio between % ISOP complexed (total oil–surface oil) under % ISOP uncomplexed (surface oil). Data obtained through GC/MS analyses

ISOP. This value represents the ratio between the percentages of ISOP complexed (total oil–adsorbed oil) and non-complexed (adsorbed oil) ISOP. The samples with β-CD exhibit the highest complexation ratio (68.3 %). These results confirm that the best inclusion procedure was PC and SC for α-CD and β-CD, respectively. The GC results corroborate the results obtained by the TG. Indeed PM not favors the complexation of ISOP (Table 1). TG results show that the PC and SC complexation methods were able to increase the ISOP content (Complex ISOP/ %) in the cavity compared to PM. This increase can be seen in the percentage of mass loss on the second stage of complex decomposition (Δm 2/%—111–293 °C), which was confirmed by the GC results (Table 1).

Fourier transform infrared (FT-IR) spectroscopy

The FT-IR spectra of all the samples (ISOP, α-CD, β-CD, PM/α-CD, PC/α-CD, SC/α-CD, PM/β-CD, PC/β-CD and SC/β-CD) are presented in Fig. 3. FT-IR spectra of ISOP consisted of the prominent absorption bands at 3495–3307 cm^{-1} ascribed O–H stretching vibrations. Between 2944 and 2838 cm^{-1} bands, the absorption was related to C–H stretching. The 1642-cm^{-1} band indicated the presence of stretching or C=C deformation, characteristic of an alkene group. At 1378 cm^{-1} region the deformation CH_3, was detected. It is note that a band approximately at 1031 cm^{-1} was related to the vibration mode of the C–O stretching. The band observed at 891 cm^{-1} corresponds to the stretching of $R_2C{=}CH_2$.

The FT-IR spectrum of α-CD (Fig. 3a) showed a high absorption at 3389 cm^{-1} for the stretching vibrations of the hydroxyl groups presented in this molecule. The band observed at 1637 cm^{-1} is also related to the presence of O–H groups. At 2920-cm^{-1} region, the band correspond to the C–H stretching, and at 1409, 1359, 1329, 1293 e 1242 cm^{-1} the bands were associated to the CH_2 and CH stretching. Other bands (1150, 1182 and 1034 cm^{-1}) were also observed and attributed to the C–O stretching, probably related to the hydroxyl and ether groups presented in the α-CD. Typical bands at 1034–706-cm^{-1} region were characteristic of C–H bond vibration and C–C skeleton, which belong to the glucopyranose ring [50].

The FT-IR spectrum of β-CD showed a prominent absorption band at 3341 cm^{-1} (credited to the O–H stretching vibrations). Another, band at 1647 cm^{-1} was also related to the O–H groups. Other bands were found at 2926 cm^{-1} region (for C–H vibrations, and C–H, C–H_2 stretching), at 1411, 1368, 1335, 1301 and 1246 cm^{-1} region (for C–H stretching), at 1154, 1080 and 1027 cm^{-1} (for C–O stretching from ether and hydroxyl groups) and at 1000–700 cm^{-1} (for C–H bonds vibration and C–C skeleton, related to the glucopyranose ring). Similar results through technique were found by Menezes et al., Menezes et al. and Sambasevam et al., suggesting the complexation of geraniol, linalool and azomethine, respectively [17, 18, 51].

The inclusion complex spectra of α-CD/ISOP and β-CD/ISOP showed alkene vibration at the 944 cm^{-1} band, the most significant band, characteristic of deformation out of plane, indicating the presence of ISOP in the complexes. In all α-CD spectra, as in the β-CD, there were some changes due to the formation of hydrogen bonds between the molecule of ISOP and β-CD.

However, the relative intensities of the PM presented a similar spectrum compared to the α-CD and the β-CD

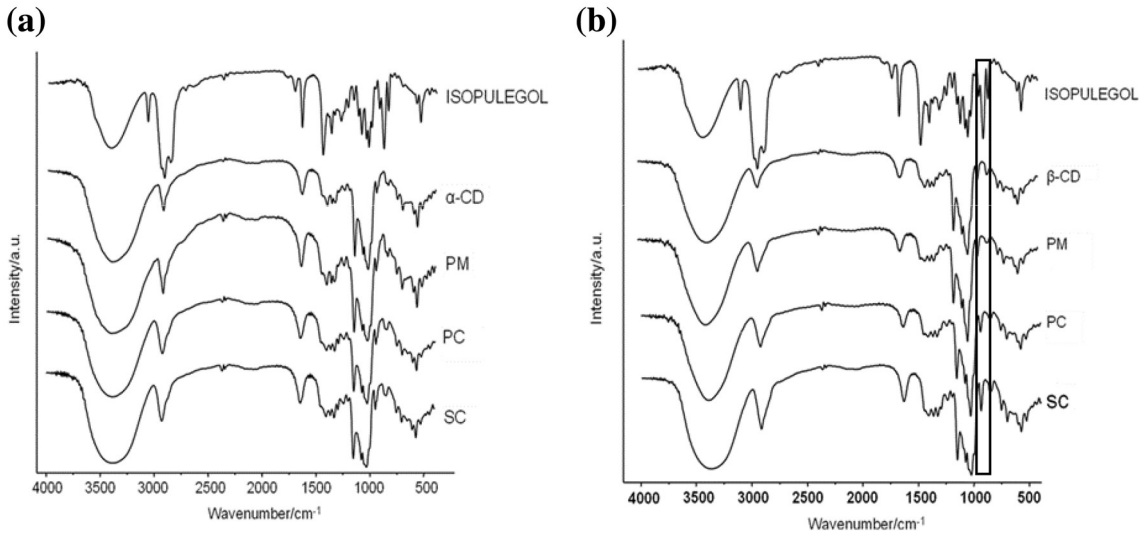

Fig. 3 FTIR spectra of ISOP, α-CD (**a**), β-CD (**b**), physical mixture (PM) and inclusion complex prepared through paste complex (PC) and slurry complex (SC)

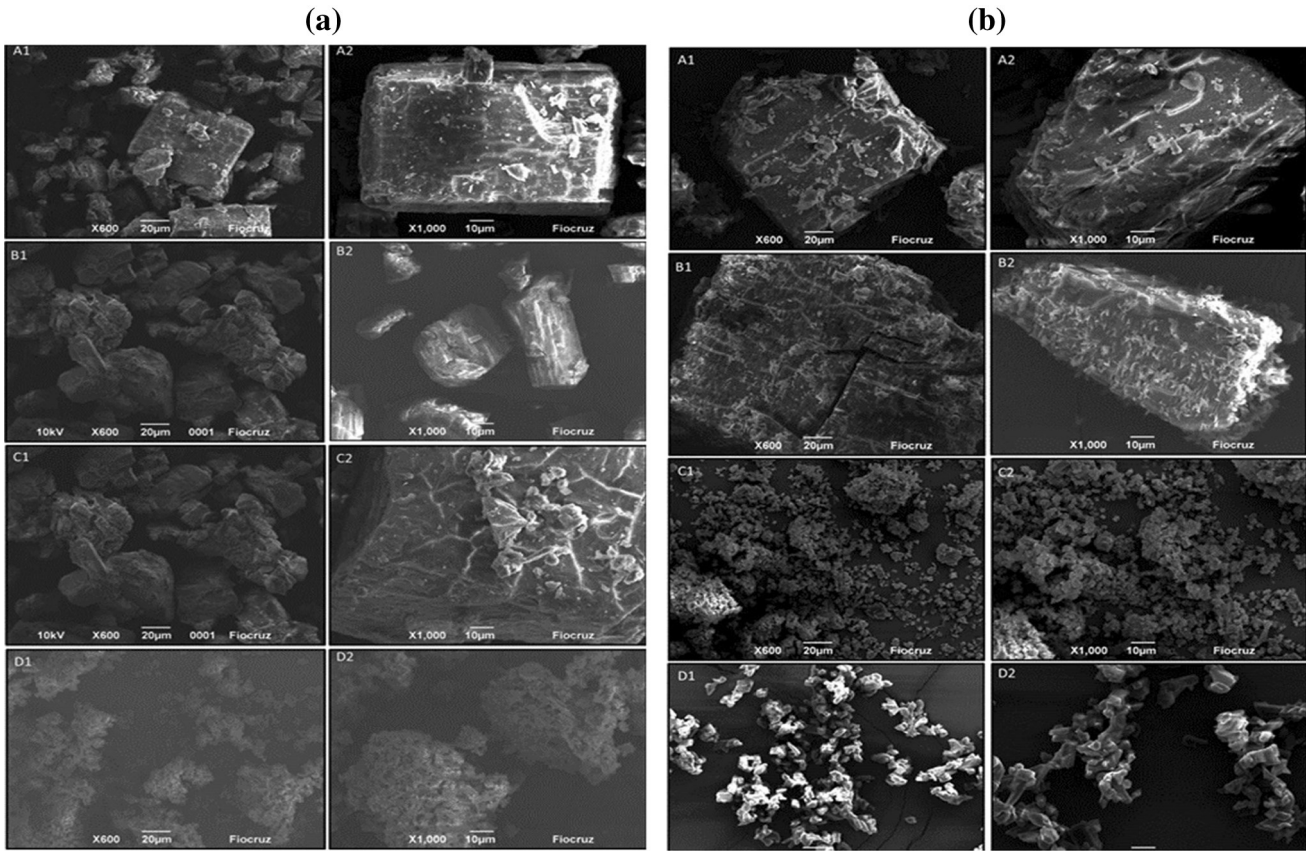

Fig. 4 SEM micrographs of cross sections (×600 and ×1000). **a** (*A*) α-CD, (*B*) physical mixture, (*C*) paste complex and (*D*) slurry complex. **b** (*A*) β-CD, (*B*) physical mixture, (*C*) paste complex and (*D*) slurry complex

bands. The PC and SC methods showed a quite similar FT-IR spectrum with large band at 1648 and at 2927 cm^{-1}, and high intensity at 944 cm^{-1}. Therefore, both methods, revealed to be quite reliable to produce α-CD/ISOP (Fig. 3a). The intensity of the bands observed in the spectra that match the inclusion complexes prepared with β-CD

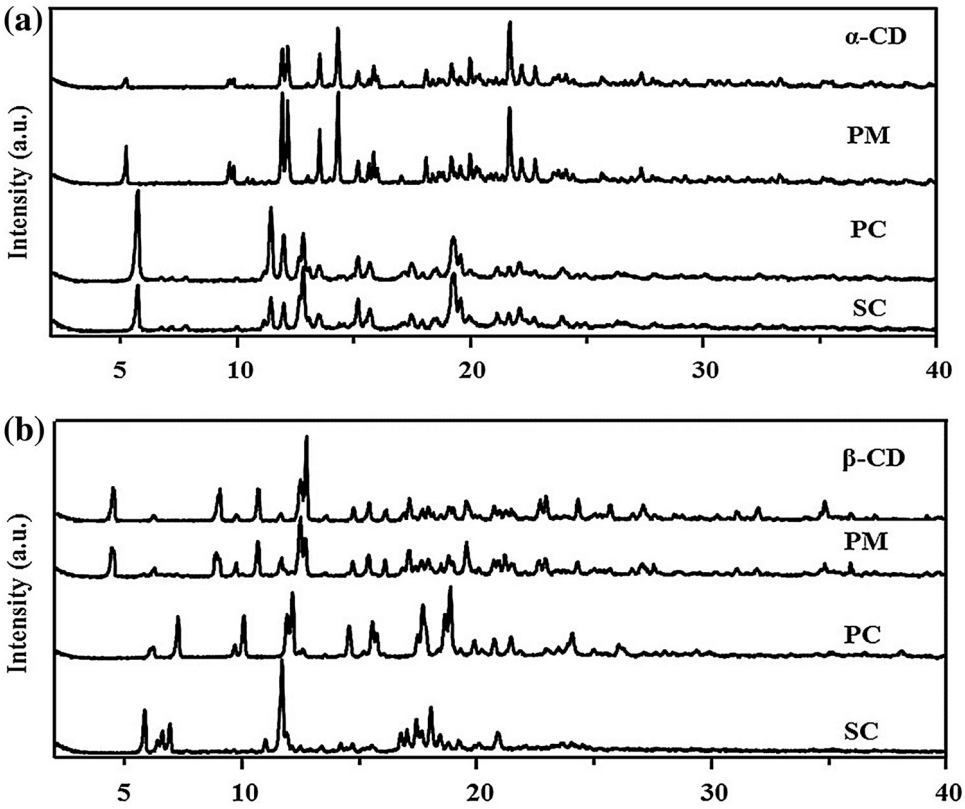

Fig. 5 Ray-diffraction of α-CD (**a**), β-CD (**b**) and samples prepared through three different methods, physical mixture (PM), paste complex (PC) and slurry complex (SC)

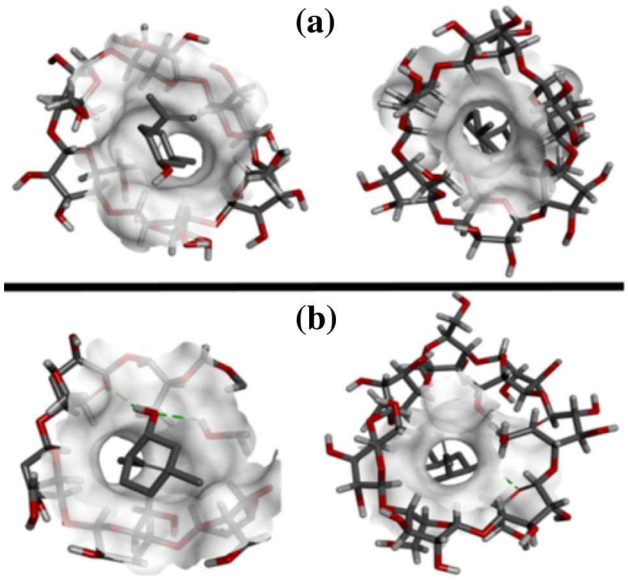

Fig. 6 The minimum energy conformation of ISOP with **a** α-CD and **b** β-CD obtained from docking simulations. The *dashed lines* represent the hydrogen bonds interactions and the *white surfaces* represent solvent accessibility surfaces

obtained through the PM and PC methods presented characteristics similar to the β-CD spectrum (Fig. 3b). However, the SC/β-CD inclusion complexes showed an increase in the intensity of the band observed at 932 cm^{-1}. Therefore, SC, was the best method to form ISOP/β-CD inclusion complex.

Scanning electron microscopy (SEM)

The SEM images of α-CD, β-CD, PM and the inclusion complexes prepared through the PC and the SC methods are presented in Fig. 4a, b, respectively. Both CDs were composed of square- and rectangular-shaped crystals forms with different sizes. On the other hand, the SEM images showed that the structure and the shape of the complexes produced by PC and SC methods were different. Figure 4a shows α-CD and its inclusion complex. It can be noticed important changes on the shape and appearance between them. Moreover, the SC method showed reduced size particle and not defined form. Figure 4b, indeed, showed changes on the shape and appearance induced by β-CD during the complex formation. PC/β-CD and SC/β-CD methods revealed form with small dimensions. However, for both α-CD and β-CD the particle shapes and morphology of the corresponding PM were quite similar to those molecules, respectively.

X-ray diffractometry (XRD)

The X-ray diffraction profile of α-CD, β-CD, PM, PC and SC are shown in Fig. 5. Some sharp diffraction lines at the

Table 2 Proton chemical shift data (ppm) of ISOP and β-CD (A) e (B) α-CD in the free state, complex (SC and PC) and physical mixture (PM) in D_2O solution (B)

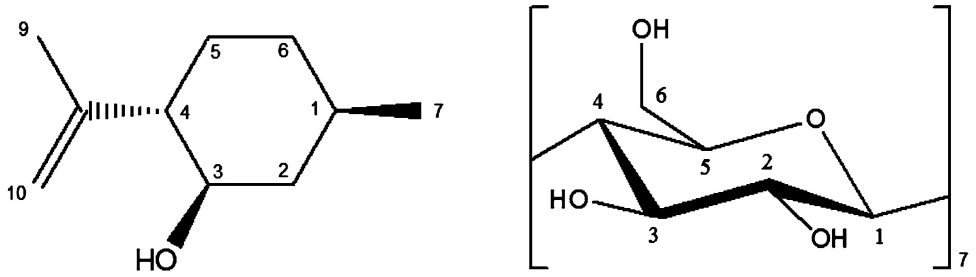

	δ Free	δ SC	δ PC	δ PM	Δδ SC	Δδ PC	Δδ PM
A							
ISOP protons							
H-10*Z*	4.82	4.93	4.91	4.96	0.11	0.09	0.14
H-10*E*	4.80	4.82	4.82	4.85	0.02	0.02	0.05
H-3	3.57	3.50	3.51	3.50	−0.07	−0.06	−0.07
H-2*eq*	1.93	2.05	2.05	2.07	0.12	0.12	0.14
H-4	1.91	1.86	1.87	1.86	−0.05	−0.04	−0.05
H-5*eq*	1.63	1.77	1.78	1.80	0.14	0.15	0.17
H-9	1.66	1.73	1.73	1.74	0.07	0.07	0.08
H-6*eq*	1.58	1.65	1.66	1.66	0.07	0.08	0.08
H-5*ax*	1.33	1.34	1.37	1.37	0.01	0.04	0.04
H-1	1.46	1.31	1.33	1.34	−0.15	−0.13	−0.12
H-2*ax*	0.91	0.94	0.94	0.94	0.03	0.03	0.03
H-7	0.87	0.86	0.87	0.86	−0.01	0.00	−0.01
H-6*ax*	0.82	0.80	0.80	0.79	−0.02	−0.02	−0.03
β-CD protons							
H-1	5.05	5.02	5.06	5.02	−0.03	0.01	−0.03
H-3	3.95	3.89	3.93	3.90	−0.06	−0.02	−0.05
H-6	3.86	3.83	3.87	3.83	−0.03	0.01	−0.03
H-5	3.84	3.74	3.79	3.80	−0.10	−0.05	−0.04
H-2	3.63	3.60	3.64	3.60	−0.03	0.01	−0.03
H-4	3.57	3.54	3.59	3.54	−0.03	0.02	−0.03
B							
ISOP protons							
H-10*Z*	4.82	4.86	4.84	4.83	0.04	0.02	0.01
H-10*E*	4.80	4.79	4.78	4.78	−0.01	−0.02	−0.02
H-3	3.57	3.62	3.59	3.39	0.05	0.02	−0.18
H-2*eq*	1.93	2.08	2.06	2.02	0.15	0.13	0.09
H-4	1.91	1.99	1.97	1.92	0.08	0.06	0.01
H-5*eq*	1.63	1.80	1.78	1.85	0.17	0.15	0.22
H-9	1.66	1.73	1.70	1.74	0.07	0.04	0.08
H-6*eq*	1.58	1.69	1.54	1.70	0.11	−0.04	0.12
H-5*ax*	1.33	1.56	1.67	1.53	0.23	0.34	0.20
H-1	1.46	1.41	1.39	1.36	−0.05	−0.07	−0.10
H-2*ax*	0.91	1.05	1.03	1.05	0.14	0.12	0.14
H-7	0.87	0.98	0.96	0.98	0.11	0.09	0.11
H-6*ax*	0.82	0.98	0.96	0.93	0.16	0.14	0.11
					0.04		

Table 2 continued

	δ Free	δ SC	δ PC	δ PM	Δδ SC	Δδ PC	Δδ PM
α-CD protons							
H-1	5.01	5.03	5.01	5.01	0.02	0.00	0.00
H-3	3.94	3.96	3.94	3.94	0.02	0.00	0.00
H-6	3.86	3.88	3.85	3.86	0.02	−0.01	0.00
H-5	3.81	3.82	3.80	3.81	0.01	−0.01	0.00
H-2	3.59	3.61	3.59	3.59	0.02	0.00	0.00
H-4	3.54	3.57	3.54	3.57	0.03	0.00	0.03

SC slurry complexation, *PC* paste complexation, *PM* physical mixture

angle of 2θ 4.76, 6.12, 9.02, 10.72, 13.98 and 20.70 were presented in the X-ray diffractogram of α-CD (Fig. 5a) and β-CD (Fig. 5b), respectively, which shows that they were crystalline compounds.

CD/ISOP PM prepared with α-CD and β-CD follow the same trend of profile, which confirms the low degree of complexation revealed by the DSC and TG studies. However, SC/α-CD and SC/β-CD, especially, showed a reduction in the number of these diffraction lines suggesting the formation of an amorphous material, predicting that those would be a more soluble material.

Molecular docking between α-, β-CD and ISOP

According to the in silico data (Fig. 6), the α-CD formed more stable inclusion complex with lower energy when compared to β-CD. This result indicates that lower affinity energy suggests stronger binding as described by Ren et al. [52]. Thus, the score observed was the most stable $\Delta E = -4.53$ kcal mol^{-1} for the inclusion complex with α-CD and the less stable for the β-CD/ISOP complex (with $\Delta E = -4.13$ kcal mol^{-1}). Therefore, it can be speculated that the internal space of the cavities influences on the interactions. The smallest cavity of the α-CD (0.5–0.6 nm) compared to the one of the β-CD (0.6–0.8 nm) facilitates the closeness of atoms, and consequently, the formation of steric, mainly, but also hydrogen bonds that corroborates with the ΔH value. Negative values of ΔH indicated hydrophobic non-covalent interactions, which may be stabilized by hydrogen bonding, as it was confirmed by the molecular docking [53, 54]. The Fig. 6 shows that ISOP fits into the cavity of α-CD in the opposite position of β-CD. Indeed, the propenyl group of ISOP is totally inside the cavity in the former, unlike in the latter, in which the methyl group of ISOP is inserted together with the cyclohexanol group. The solvent accessibility surface aids the visualization of the bigger cavity of β-CD, and that ISOP fits better in the smallest cavity of α-CD.

Nuclear magnetic resonance

1D and 2D ^{1}H NMR analyses were used to study the inclusion complex formation in solution phases. The chemical shift changes shown by ISOP and β-CD protons in the complexes prepared through the three inclusion complex methods (PM, PC and SC) suggest inclusion process by non-covalent interactions (Table 2). Figure 7a illustrates partial ^{1}H NMR of free ISOP and β-CD/ISOP (SC method) in which H-10*Z*, H-10*E,* H-2*eq*, H-5*eq*, H-9, H-6*eq*, H-5*ax* and H-2*ax* protons of ISOP are influenced due to the presence of β-CD. The upfield shift of the H-3 and the H-5 β-CD cavity protons gives clear evidence of the formation of the inclusion complex (Fig. 7b). To obtain further information on the inclusion complexation, 2D ROESY experiment was carried out. Figure 7c shows the evidence of spatial proximities between aliphatic protons of ISOP and β-CD [55]. Intermolecular cross-peaks were observed between protons of the ISOP (H-2*eq*, H-5*eq*, H9, H-6*eq*, H1, H-5*ax*, H-2*ax*, H7, H-6*ax*) and the H-3 and H-5 protons of β-CD. An Additional dipolar correlation was observed between H-10*E*, H-10*Z* and H-4 protons of ISOP and the H-3 of β-CD. The same described intermolecular cross-peaks were observed with β-CD/ISOP complex prepared by the PC and PM methods.

For α-CD/ISOP complexes (SC and PC methods) the ^{1}H NMR aliphatic region was assigned with the help of COSY data, due to the separation between the signals of H-2*eq* and H-4 from the complex (SC and PC methods) comparing to the same signals of free ISOP, which were overlapping (Fig. 7d). ISOP protons are influenced by the presence of α-CD (Fig. 7d; Table 2). On the other hand, no great chemical shift variation in the α-CD region was observed. In 2D ROESY spectra, intermolecular cross-peaks were observed between the H-3 proton of the α-CD and the protons of the ISOP (H-2eq, H4, H-5eq, H9, H-6eq, H1, H-5ax, H-2ax, H7, H-6ax). Moreover, one interaction between the H-7 of the ISOP and the H-5 of the α-CD confirmed the inclusion (Fig. 7e). This is the proof of concept that ISOP was able to

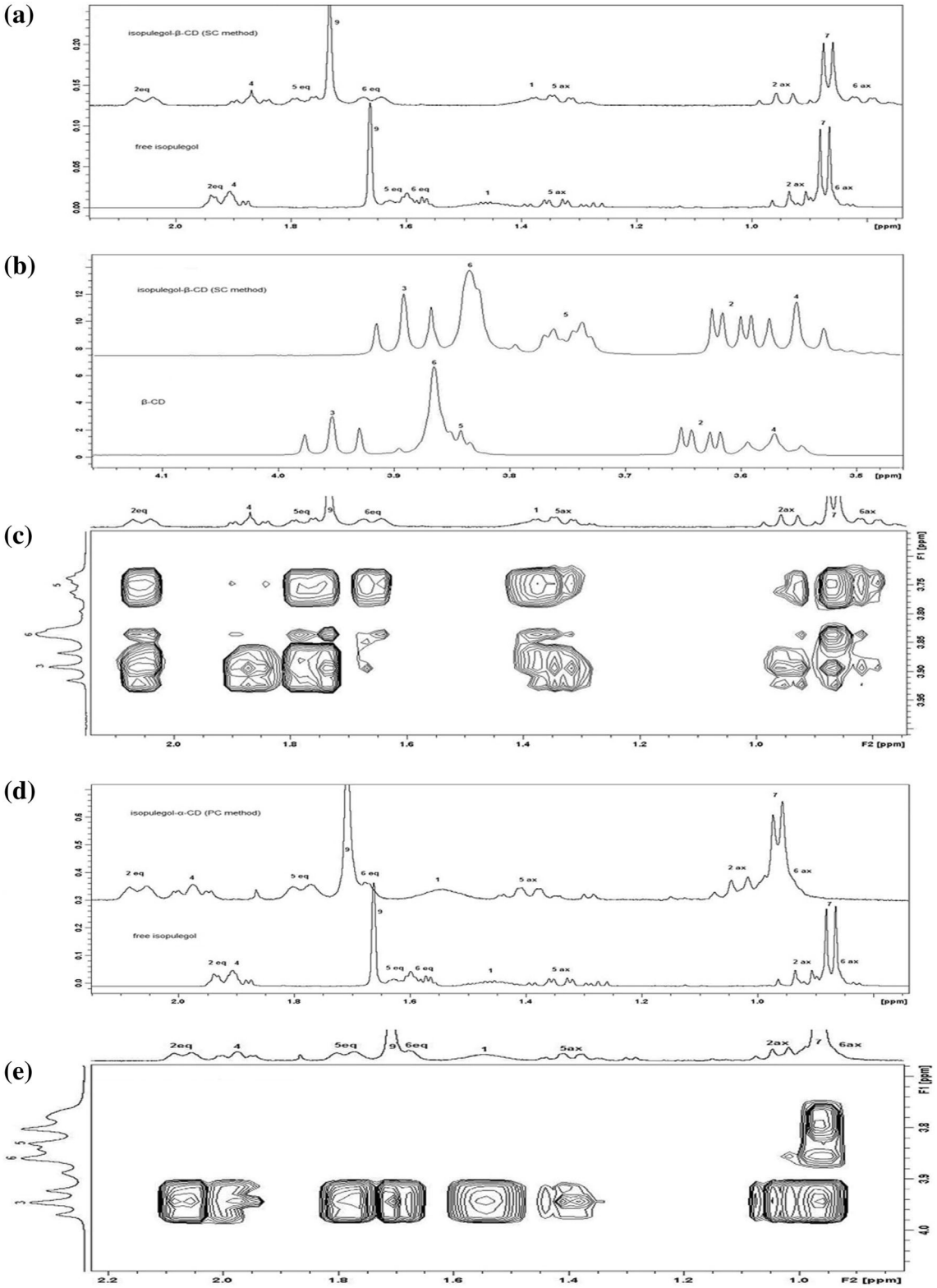

Fig. 7 **a** Partial ^{1}H NMR of ISOP-β-CD complex by slurry complexation (SC, **a**) and free ISOP (**b**) in D_2O, showing chemical shifts changes in aliphatic region. **b** Partial ^{1}H NMR of ISOP-β-CD complex by slurry complexation (SC) and β-CD in D_2O, showing changes of chemical shifts in H-3, H-6, H-5, H-2 and H-4 β-CD protons. **c** Partial 2D ROESY of ISOP-β-CD complex (SC method) in D_2O. **d** Partial ^{1}H NMR of ISOP-α-CD complex by slurry complexation (SC) and free ISOP in D_2O, showing chemical shifts changes in aliphatic region. **e** Partial 2D ROESY of ISOP-α-CD complex (PC method) in D_2O

reach inside the cavity of α-CD through the SC and the PC complexation methods. These results are not in accordance to the ones of Ceborska et al. who stated that the cavity of α-CD was not large enough for the incorporation of ISOP molecules [56]. Only for PM, no significant chemical shift changes in ^{1}H NMR or intermolecular cross-peaks were observed, suggesting that for this methodology of complexation, ISOP is not included inside the α-CD.

Conclusion

The results showed that α-CD and β-CDs were able to produce inclusion complexes of ISOP, which can be credited to the cavity size of CDs and its affinity for ISOP. Furthermore, the physicochemical characterization indicates that the best inclusion complexes were created through the PC/α-CD and SC/β-CD methods. 1D and 2D ^{1}H NMR provided a good description of the inclusion model and spatial conformation of β-CD/ISOP and α-CD/ISOP inclusion complex. Chemical shift changes and intermolecular cross-peaks observed between protons of ISOP and CDs suggest the formation of an inclusion process by non-covalent interactions, except for PM using α-CD.

Acknowledgments The authors are grateful to CAPES, CNPq, FINEP and FAPITEC/SE for the financial support and fellowships. We thank M. L. V. Moreno, C. P. Figueira and Prof. A. L. Rangel for the images of SEM made in the Gonçalo Moniz Research Center, at the Oswaldo Cruz Foundation.

Compliance with ethical standards

Conflict of interest The authors have declared that there is no conflict of interest.

References

1. de Sousa, D.P.: Analgesic-like activity of essential oils constituents. Molecules **16**(3), 2233–2252 (2011). doi:10.3390/molecules16032233
2. Guimarães, A.G., Serafini, M.R., Quintans Jr., L.J.: Terpenes and derivatives as a new perspective for pain treatment: a patent review. Expert Opin. Ther. Patents **24**, 1–23 (2013)
3. Degenhardt, J., Kollner, T.G., Gershenzon, J.: Monoterpene and sesquiterpene synthases and the origin of terpene skeletal diversity in plants. Phytochemistry **70**(15–16), 1621–1637 (2009). doi:10.1016/j.phytochem.2009.07.030
4. Silva, M.I., de Aquino Neto, M.R., Neto, P.F.T., Moura, B.A., do Amaral, J.F., de Sousa, D.P., Vasconcelos, S.M.M., de Sousa, F.C.F.: Central nervous system activity of acute administration of isopulegol in mice. Pharmacol. Biochem. Behav. **88**(2), 141–147 (2007). doi:10.1016/j.pbb.2007.07.015
5. Lenardão, E.J., Botteselle, G.V., Azambuja, F., Perin, G., Jacob, R.G.: Citronellal as key compound in organic synthesis. Tetrahedron **63**, 6671–6712 (2007)
6. Silva, M.I., Silva, M.A., de Aquino Neto, M.R., Moura, B.A., de Sousa, H.L., de Lavor, E.P., de Vasconcelos, P.F., Macedo, D.S., de Sousa, D.P., Vasconcelos, S.M., de Sousa, F.C.: Effects of isopulegol on pentylenetetrazol-induced convulsions in mice: possible involvement of GABAergic system and antioxidant activity. Fitoterapia **80**(8), 506–513 (2009). doi:10.1016/j.fitote.2009.06.011
7. Bhatia, S.P., McGinty, D., Letizia, C.S., Api, A.M.: Fragrance material review on isopulegol. Food Chem. Toxicol. **46**(Suppl 11), S185–S189 (2008). doi:10.1016/j.fct.2008.06.053
8. Belsito, D., Bickers, D., Bruze, M., Calow, P., Greim, H., Hanifin, J.M., Rogers, A.E., Saurat, J.H., Sipes, I.G., Tagami, H.: A toxicologic and dermatologic assessment of cyclic and non-cyclic terpene alcohols when used as fragrance ingredients. Food chem. Toxicol. **46**(Suppl 11), S1–S71 (2008). doi:10.1016/j.fct.2008.06.085
9. Ishida, K., Obata, Y., Takayama, K.: Transdermal absorption promoter, and external skin formulation thereof. In: Google Patents (2013)
10. Chen, Y., Cun, D., Quan, P., Liu, X., Guo, W., Peng, L., Fang, L.: Saturated long-chain esters of isopulegol as novel permeation enhancers for transdermal drug delivery. Pharm. Res. **31**(8), 1907–1918 (2014). doi:10.1007/s11095-013-1292-0
11. Chen, Y., Quan, P., Liu, X., Guo, W., Song, W., Cun, D., Wang, Z., Fang, L.: Enhancement of skin permeation of flurbiprofen via its transdermal patches using isopulegol decanoate (ISO-C10) as an absorption enhancer: pharmacokinetic and pharmacodynamic evaluation. J. Pharm. Pharmacol. **67**(9), 1232–1239 (2015). doi:10.1111/jphp.12428
12. Hamoudi, M.C., Bourasset, F., Domergue-Dupont, V., Gueutin, C., Nicolas, V., Fattal, E., Bochot, A.: Formulations based on alpha cyclodextrin and soybean oil: an approach to modulate the oral release of lipophilic drugs. J. Controll. Release **161**(3), 861–867 (2012). doi:10.1016/j.jconrel.2012.05.032
13. Savjani, K.T., Gajjar, A.K., Savjani, J.K.: Drug solubility: importance and enhancement techniques. ISRN Pharm. **2012**, 195727 (2012). doi:10.5402/2012/195727
14. Venturini, C.G., Jäger, E., Oliveira, C.P., Bernardi, A., Battastini, A.M.O., Guterres, S.S., Pohlmann, A.R.: Formulation of lipid core nanocapsules. Colloids Surf. A **375**(1–3), 200–208 (2011). doi:10.1016/j.colsurfa.2010.12.011
15. Danhier, F., Ansorena, E., Silva, J.M., Coco, R., Le Breton, A., Préat, V.: PLGA-based nanoparticles: an overview of biomedical applications. J. Controll. Release **161**(2), 505–522 (2012). doi:10.1016/j.jconrel.2012.01.043
16. Rassu, G., Soddu, E., Cossu, M., Brundu, A., Cerri, G., Marchetti, N., Ferraro, L., Regan, R.F., Giunchedi, P., Gavini, E., Dalpiaz, A.: Solid microparticles based on chitosan or methyl-β-cyclodextrin: a first formulative approach to increase the nose-to-brain transport of deferoxamine mesylate. J. Controll. Release **201**, 68–77 (2015). doi:10.1016/j.jconrel.2015.01.025
17. Menezes, P.P., Serafini, M.R., Santana, B.V., Nunes, R.S., Quintans, L.J., Silva, G.F., Medeiros, I.A., Marchioro, M., Fraga, B.P., Santos, M.R., Araújo, A.A.: Solid-state β-cyclodextrin complexes containing geraniol. Thermochim. Acta **548**, 45–50 (2012)
18. Menezes, P.P., Serafini, M.R., Quintans-Júnior, L.J., Silva, G.F., Oliveira, J.F., Carvalho, F.M.S., Souza, J.C.C., Matos, J.R., Alves, P.B., Matos, I.L., Hădărugă, D.I., Araújo, A.A.S.: Inclusion complex of (-)-linalool and b-cyclodextrin. J. Therm. Anal. Calorim. **115**, 2429–2437 (2014)
19. Menezes Pdos, P., Araujo, A.A., Doria, G.A., Quintans-Junior, L.J., de Oliveira, M.G., dos Santos, M.R., de Oliveira, J.F., Matos Jdo, R., Carvalho, F.M., Alves, P.B., de Matos, I.L., dos Santos, D.A., Marreto, R.N., da Silva, G.F., Serafini, M.R.: Physicochemical characterization and analgesic effect of inclusion complexes of essential oil from *Hyptis pectinata* L. Poit leaves with beta-cyclodextrin. Current Pharm. Biotechnol. **16**(5), 440–450 (2015)

20. Pinho, E., Grootveld, M., Soares, G., Henriques, M.: Cyclodextrins as encapsulation agents for plant bioactive compounds. Carbohydr. Polym. **101**, 121–135 (2014). doi:10.1016/j.carbpol.2013.08.078
21. Loftsson, T., Brewster, M.E.: Pharmaceutical applications of cyclodextrins: basic science and product development. J. Pharm. Pharmacol. **62**(11), 1607–1621 (2010). doi:10.1111/j.2042-7158.2010.01030.x
22. Kurkov, S.V., Loftsson, T.: Cyclodextrins. Int. J. Pharm. **453**, 167–180 (2013)
23. Crini, G.: Review: a history of cyclodextrins. Chem. Rev. **114**(21), 10940–10975 (2014). doi:10.1021/cr500081p
24. Jambhekar, S.S., Breen, P.: Cyclodextrins in pharmaceutical formulations I: structure and physicochemical properties, formation of complexes, and types of complex. Drug Discov. Today **21**(2), 356–362 (2016). doi:10.1016/j.drudis.2015.11.017
25. Jambhekar, S.S., Breen, P.: Cyclodextrins in pharmaceutical formulations II: solubilization, binding constant, and complexation efficiency. Drug Discov. Today **21**(2), 363–368 (2016). doi:10.1016/j.drudis.2015.11.016
26. Valente, A.J.M., Söderman, O.: The formation of host–guest complexes between surfactants and cyclodextrins. Adv. Colloid Interface Sci. **205**, 156–176 (2014). doi:10.1016/j.cis.2013.08.001
27. Marques, H.M.C.: A review on cyclodextrin encapsulation of essential oils and volatiles. Flavour Frag. J. **25**, 313–326 (2010)
28. Marreto, R.N., Almeida, E.E.C.V., Alves, P.B., Niculau, E.S., Nunes, R.S., Matos, C.R.S., Araújo, A.A.S.: Thermal analysis and gas chromatography coupled mass spectrometry analyses of hydroxypropyl-β-cyclodextrin inclusion complex containing Lippia gracilis essential oil. Thermochim. Acta **475**, 53–58 (2008)
29. Allinger, N.L.: A hydrocarbon force-field utilizing V1 and V2 torsional terms. J. Am. Chem. Soc. **99**, 8127–8134 (1977)
30. Dewar, M.J.S.E., Zoebisch, G., Healy, E.F.: AM., S.J.J.P.: A new general purpose quantum mechanical molecular model. J. Am. Chem. Soc. **107**, 3902–3909 (1985)
31. Cohen, N.C.: Guidebook on molecular modeling in drug design. Academic Press, San Diego (1996)
32. Leach, A.R.: Molecular modeling: principles and applications. Prentice Hall, London (2001)
33. Molegro. http://www.clcbio.com/products/molegro/#molecular-viewer. Accessed 14 Aug 2013
34. Wolf, L.K.: New software and websites for the chemical enterprise. Chem. Eng. News **87**, 31 (2009)
35. Priotti, J., Ferreira, M.J., Lamas, M.C., Leonardi, D., Salomon, C.J., Nunes, T.G.: First solid-state NMR spectroscopy evaluation of complexes of benznidazole with cyclodextrin derivatives. Carbohydr. Polym. **131**, 90–97 (2015). doi:10.1016/j.carbpol.2015.05.045
36. Hădărugă, D.I., Ünlüsayin, M., Gruia, A.T., Birău, C., Rusu, G., Hădărugă, N.G.: Thermal and oxidative stability of Atlantic salmon oil (Salmo salar L.) and complexation with β-cyclodextrin. Beilstein J. Org. Chem. **12**, 179–191 (2016). doi:10.3762/bjoc.12.20
37. Giordano, F., Novak, C., Moyano, J.: Thermal analysis of cyclodextrins and their inclusion compounds. Thermochim. Acta **380**, 123–151 (2001)
38. Prabu, S., Sivakumar, K., Swaminathan, M., Rajamohan, R.: Preparation and characterization of host–guest system between inosine and β-cyclodextrin through inclusion mode. Spectrochim. Acta A **147**, 151–157 (2015). doi:10.1016/j.saa.2015.03.056
39. Wang, X., Luo, Z., Xiao, Z.: Preparation, characterization, and thermal stability of β-cyclodextrin/soybean lecithin inclusion complex. Carbohydr. Polym. **101**, 1027–1032 (2014). doi:10.1016/j.carbpol.2013.10.042
40. Zhang, W., Li, X., Yu, T., Yuan, L., Rao, G., Li, D., Mu, C.: Preparation, physicochemical characterization and release behavior of the inclusion complex of trans-anethole and β-cyclodextrin. Food Res. Int. **74**, 55–62 (2015). doi:10.1016/j.foodres.2015.04.029
41. Rajendiran, N., Mohandoss, T., Venkatesh, G.: Investigation of inclusion complexes of sulfamerazine with α- and β-cyclodextrins: An experimental and theoretical study. Spectrochim. Acta A **124**, 441–450 (2014). doi:10.1016/j.saa.2014.01.057
42. Castronuovo, G., Niccoli, M.: Thermodynamics of inclusion complexes of natural and modified cyclodextrins with acetylsalicylic acid and ibuprofen in aqueous solution at 298 K. Thermochim. Acta **557**, 44–49 (2013). doi:10.1016/j.tca.2013.01.037
43. Rajendiran, N., Siva, S.: Inclusion complex of sulfadimethoxine with cyclodextrins: Preparation and characterization. Carbohydr. Polym. **101**, 828–836 (2014). doi:10.1016/j.carbpol.2013.10.016
44. Kohata, S., Jyodoi, K., Ohyoshi, A.: Thermal decomposition of cyclodextrins (α-, β-, γ-, and modified β-CyD) and of metal-(β-CyD) complexes in the solid phase. Thermochim. Acta **217**, 187–198 (1993)
45. Serafini, M.R., Menezes, P.P., Costa, L.P., Lima, C.M., Quintans Jr., L.J., Cardoso, J.C., Matos, J.R., Soares-Sobrinho, J.L., Grangeiro Jr., S., Nunes, P.S., Bonjadim, L.R., Araújo, A.A.S.: Interaction of p-cymene with β-cyclodextrin. J. Therm. Anal. Calorim. (2011). doi:10.1007/s10973-011-1736
46. Hădărugă, N.G., Hădărugă, D.I., Isengard, H.Z.: Water content of natural cyclodextrins and their essential oil complexes: a comparative study between Karl Fischer titration and thermal methods. Food Chem. **132**, 1741–1748 (2012)
47. Wu, H., Liang, H., Yuan, Q., Wang, T., Yan, X.: Preparation and stability investigation of the inclusion complex of sulforaphane with hydroxypropyl-β-cyclodextrin. Carbohydr. Polym. **82**(3), 613–617 (2010). doi:10.1016/j.carbpol.2010.05.020
48. dos Santos, C., Buera, M.D.P., Mazzobre, M.F.: Phase solubility studies of terpineol with β-cyclodextrins and stability of the freeze-dried inclusion complex. Proced. Food Sci. **1**, 355–362 (2011). doi:10.1016/j.profoo.2011.09.055
49. Valle, M.D.: Cyclodextrins and their uses: a review. Process Biochem. **5**, 1033–1046 (2004)
50. Rajendiran, N., Siva, S., Saravanan, J.: Inclusion complexation of sulfapyridine with α- and β-cyclodextrins: spectral and molecular modeling study. J. Mol. Struct. **1054–1055**, 215–222 (2013)
51. Sambasevam, K.P., Mohamad, S., Sarih, N.M., Ismail, N.A.: Synthesis and characterization of the inclusion complex of beta-cyclodextrin and azomethine. Int. J. Mol. Sci. **14**(2), 3671–3682 (2013). doi:10.3390/ijms14023671
52. Ren, J., Yao, P., Cao, Y., Cao, J., Zhang, L., Wang, Y., Jia, L.: Application of cyclodextrin-based eluents in hydrophobic charge-induction chromatography: elution of antibody at neutral pH. J. Chromatogr. A **1352**, 62–68 (2014). doi:10.1016/j.chroma.2014.05.060
53. Budryn, G., Pałecz, B., Rachwał-Rosiak, D., Oracz, J., Zaczyńska, D., Belica, S., Navarro-González, I., Meseguer, J.M.V., Pérez-Sánchez, H.: Effect of inclusion of hydroxycinnamic and chlorogenic acids from green coffee bean in β-cyclodextrin on their interactions with whey, egg white and soy protein isolates. Food Chem. **168**, 276–287 (2015). doi:10.1016/j.foodchem.2014.07.056
54. Medarević, D., Kachrimanis, K., Djurić, Z., Ibrić, S.: Influence of hydrophilic polymers on the complexation of carbamazepine with hydroxypropyl-β-cyclodextrin. Eur. J. Pharm. Sci. **78**, 273–285 (2015). doi:10.1016/j.ejps.2015.08.001
55. Meinguet, C., Masereel, B., Wouters, J.: Preparation and characterization of a new harmine-based antiproliferative compound in complex with cyclodextrin: increasing solubility while maintaining biological activity. Eur. J. Pharm. Sci. **77**, 135–140 (2015). doi:10.1016/j.ejps.2015.06.010
56. Ceborska, M., Szwed, K., Suwinska, K.: beta-Cyclodextrin as the suitable molecular container for isopulegol enantiomers. Carbohydr. Polym. **97**(2), 546–550 (2013). doi:10.1016/j.carbpol.2013.04.097